Variable-Mass Dynamics Implementation in Multi-Physics Environment for Reusable Launcher Simulations

Björn Gäßler[(1)†], *Lâle Evrim Briese*[(1)], *Paul Acquatella*[(1)],
Pedro Simplício[(2)], *Samir Bennani*[(2)], *Massimo Casasco*[(2)]

[(1)]*DLR, German Aerospace Center, Institute of System Dynamics and Control*
Oberpfaffenhofen D-82234, Germany
{bjoern.gaessler, lale.briese, paul.acquatella}@dlr.de

[(2)]*European Space Agency ESA/ESTEC*
Noordwijk, NL-2200, The Netherlands
{pedro.simplicio, samir.bennani, massimo.casasco}@esa.int
[†]Corresponding author

Abstract

One of the driving challenges in launcher Guidance and Control (G&C) design is the strong coupling between different disciplines such as propulsion, aerodynamics, actuators, and structures, which all have a multi-physics nature. Enabling a more efficient and accurate modeling of these multi-disciplinary interactions through the use of a multi-physics modeling approach is believed to be beneficial in expediting the design process, reducing the conservatism in the assumptions used by G&C design and thereby improving the launcher performance. In particular, the accurate modeling of time-varying propellant mass dynamics is an essential component during preliminary design studies since it might have an impact on the dynamical simulations that in turn influence the assessment and evaluation of the launcher performance and trade-off designs across disciplines. This paper presents the implementation of variable-mass dynamics towards the preliminary design and development of a dedicated multi-physics simulator, termed R2M2 (*Rapid Reusable Launcher Simulation via Multi-physics Modelling*), for multi-actuated vertical take-off vertical landing (VTVL) launch vehicles. The paper first recapitulates previous investigations on variable-mass dynamics from relevant literature, including specific descriptions of the dynamical effects during translational and rotational motion. It further addresses the implementation of these dynamical effects within a multi-physics modeling environment and shows the impact of variable-mass dynamical effects on the rotational motion. The model implementation and analysis of results is performed using simple yet representative models of different burn types of propellants or engines which are commonly found in launch vehicle configurations.

1. Introduction

Ongoing demand for launch opportunities has stimulated the development of dedicated reusable launch vehicles and concepts, mainly due to the large amount of spacecraft that are rapidly increasing in development and production as evidenced in recent years. Such a large market of future satellites and space missions makes these launcher developments a highly competitive environment entailing a set of new challenges that have to be assessed rapidly and with agility. One of the driving challenges in launcher Guidance and Control (G&C) design is the strong coupling between different disciplines, such as propulsion, aerodynamics, actuators, and structure, which have a multi-physics nature. In the current industrial approach, these multi-physics effects are tackled by separate teams using their own tools, and G&C design is usually based on low-fidelity models that simplify the interactions between disciplines as discussed in [4]. Enabling a more efficient and accurate modeling of some of the multi-disciplinary interactions mentioned above through the use of a multi-physics modeling approach is believed to be beneficial in expediting the design process, reducing the conservatism in the assumptions used by G&C design as demonstrated in [1–4] and thereby improving the launcher performance.

In particular, the accurate modeling of time-varying propellant mass dynamics is an essential component during preliminary design studies since it might have an impact on the dynamical simulations that in turn influences the assessment and evaluation of the launcher performance and trade-offs across disciplines. In most simulators and studies published or described openly in the literature, variable-mass dynamics are usually simplified and considered as a linear relationship of mass flow rate which in turn only affects the mass and moment of inertia while neglecting other fundamental dynamical effects due to the mass variability itself. While this might be a valid assumption for some burn/thrust profiles, existing angular velocities of a launch vehicle can be actually damped or amplified by variable-mass dynamical effects during propellant burn as discussed in [8,9,24]. Such variable-mass dynamical effects have been addressed in literature at fundamental levels (via Lagrange and Kane's formalism, for instance) [6,7,10,12,17]. In this context, the reader is referred to [18] for a literature survey on recent investigations on the dynamics of variable-mass systems. In most cases, the variable-mass formulation is derived analytically depending on the propellant/burn profile and geometry, giving rise to equations that can be easily implemented and verified with simple models. Since it can be shown that the variable-mass dynamics in turn have an effect both on the translation and rotational motion, these effects were also included in recent framework developments for launch vehicle flight dynamics modeling and simulation [1, 3, 4, 23] as well as within nonlinear inverse models used for the control of satellites with flexible structures [21].

The objective of this paper is therefore to present the implementation of variable-mass dynamics towards the preliminary design and development of a dedicated multi-physics simulator, termed R2M2 (*Rapid Reusable Launcher Simulation via Multi-physics Modelling*), for multi-actuated vertical take-off vertical landing (VTVL) launch vehicles. In Section 2, the paper recapitulates previous investigations on variable-mass dynamics from the relevant literature, including specific descriptions of the dynamical effects during translational and rotational motion based on [6]. Subsequently, the implementation of these variable-mass dynamical effects in a modular fashion in MATLAB and Simulink [15] together with the multi-physics modeling environment Simscape [13] and Simscape Multibody [14] is described in Section 3 [1]. The implementation of launcher dynamics in Simscape and Simscape Multibody is motivated by the possibility to perform acausal modeling of components and physical models within MATLAB and Simulink, allowing to easily integrate other domains like G&C within a single environment. This line of work have been previously demonstrated in [11, 19, 22]. Additionally, the variable-mass dynamical effects are discussed in Section 4 using simple yet representative models of different burn types which can be commonly found in launch vehicle configurations. These model implementations are cross-checked and validated with theoretical results from the literature [6] as well as against alternative implementations in the multi-physics and acausal modeling language MODELICA [16] and its simulation environment DYMOLA [5]. The paper also focuses on showcasing the discrepancies arising when these variable-mass dynamical effects are neglected or not properly implemented, which in turn might have an effect on the assessment of the overall launch vehicle. Finally, in Section 5 the main contributions and conclusions are summarized, followed by an outlook towards future developments.

2. Variable-Mass System Dynamics

Modeling of variable-mass dynamics is a complex though essential component for launch vehicle simulations. Mass properties of launch vehicles are mainly changing due to the propulsion causing the ejection of combustion products from the rocket engines through their nozzles. The varying mass influences not only the vehicle's properties such as the center of mass and moments of inertia but also generates additional forces and moments for instance due to Coriolis effects. In this section, the extended equations of translational and rotational motion as well as the additional forces and moments are shown based on [6, 17]. Both apply the 'principle of solidification' which regards the variable-mass system as a constant mass system at any given point in time using its corresponding mass properties. Effects due to variable-mass dynamics are then covered by additional forces and moments. The dynamic equations of motion for these kinds of systems as obtained by [6] based on Kane's formalism are summarized within this section.

2.1 MCI Properties

The MCI properties, including mass, center of mass (CoM), and moment of inertia (MoI), are all subject to change in a variable-mass system. The most obvious is the mass itself, but also CoM and MoI change due to a different mass and mass distribution. For the investigations within this work we focus on cylindrical variable-mass bodies. This seems reasonable since most rocket solid boosters or fuel and oxidizer tanks have a cylindrical shape.

Furthermore, we consider different burn types as shown in Figure 1. These burn types can roughly be divided by their application for solid boosters or liquid fuel/oxidizer tanks. On one hand, the most common burn type for solid boosters is a *Centrifugal burn*, where the solid propellant burns from the inside outwards. Normally, the inside area

---

[1]MATLAB[®], Simulink[®], Simscape[®] and Simscape Multibody[®] are registered trademarks of MathWorks Inc.
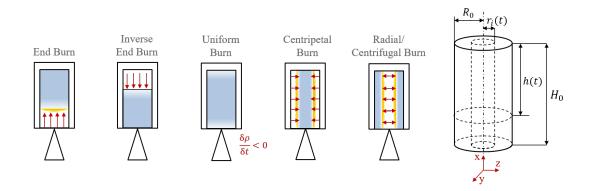
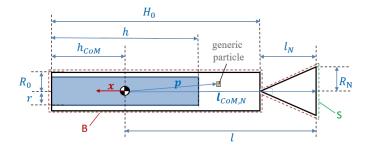Figure 1: Different burn types and geometrical properties

Figure 2: Geometrical properties including structure and nozzle

Table 1: Burn types - Calculation of properties

Burn Type	Geometry	Moment of Inertia
End Burn	$r(t) = R_0$	$I_{xx} = \frac{1}{2}m(t)R_0^2$
	$h(t) = H_0 \frac{m(t)}{m_0}$	$I_{yy} = I_{zz} = m(t)\left(\frac{1}{4}R_0^2 + \frac{1}{12}h(t)^2\right)$
Uniform Burn	$r(t) = R_0$	$I_{xx} = \frac{1}{2}m(t)R_0^2$
	$h(t) = H_0$	$I_{yy} = I_{zz} = m(t)\left(\frac{1}{4}R_0^2 + \frac{1}{12}H_0^2\right)$
Centrifugal Burn	$r_i(t) = \sqrt{R_0^2 - \frac{m(t)}{m_0}(R_0^2 - r_{0,i}^2)}$	$I_{xx} = \frac{1}{2}m(t)\left(R_0^2 + r_i(t)^2\right)$
	$r_o(t) = R_{0,o}$	$I_{yy} = I_{zz} = m(t)\left(\frac{1}{4}\left(R_0^2 + r_i(t)^2\right) + \frac{1}{12}H_0^2\right)$
	$h(t) = H_0$	
Centripetal Burn	$r_i(t) = 0$	$I_{xx} = \frac{1}{2}m(t)r(t)^2$
	$r_o(t) = \sqrt{m(t)\frac{R_0^2}{m_0}}$	$I_{yy} = I_{zz} = m(t)\left(\frac{1}{4}r(t)^2 + \frac{1}{12}H_0^2\right)$
	$h(t) = H_0$	

of the solid propellant has a complex shape for thrust curve shaping but for simplicity the shape has been assumed to be circular within the investigations of this work. Other types include the *End burn* where the propellant burns from its lower end upwards, and the uncommon *Centripetal burn* which burns from the outside towards the middle. These profiles are considered to be in the solid booster category. On the other hand, the *Uniform burn* and the Inverse End burn can be used to model liquid fuel/oxidizer tanks. For the Inverse End burn type the tank gets depleted from its top as it is often the case for pressure-fed rocket engine engines. The Uniform burn has a constant volume. If mass is lost, the density of matter inside the tank decreases. This burn type can be used to model the fuel and oxidizer tanks

for pump-fed engines. For all burn profiles the position of the CoM and the MoI changes differently when mass is depleted. Table 1 summarizes the calculation of geometrical properties and MoI for a cylindrical body when different burn types are applied. The corresponding geometrical properties and frame definition can be seen in Figures 1 and 2. The subscript 'i' means *inner*, 'o' means *outer* and '0' refers to initial values. If the body under consideration consists of several elements as shown in Figure 2, Steiner's theorem can be used to calculate the MoI for the overall body.

The changes in mass, CoM and MoI are included in almost all launch vehicle simulators in literature. However, this does not necessarily apply when it comes to the additional forces and moments due to variable-mass dynamical effects, which are described in the next sections for translational and rotational motions.

2.2 Translational Motion

The translational motion of a mass-varying body can be described as [6]

$$m\boldsymbol{a} = \boldsymbol{F}_{\text{ext}} + \boldsymbol{F}_{\text{C}} + \boldsymbol{F}_{\text{T}} + \boldsymbol{F}_{\text{L}} \tag{1}$$

where m is the body's mass, $\boldsymbol{a}$ the translational acceleration, $\boldsymbol{F}_{\text{ext}}$ are the external forces acting on the body, $\boldsymbol{F}_{\text{C}}$ the Coriolis force, $\boldsymbol{F}_{\text{T}}$ the thrust force, which is often already included in the external forces and $\boldsymbol{F}_{\text{L}}$ is a force created when the system's linear momentum changes due to particle motion within the system. A detailed derivation of these equations using Kane's formalism is described in [6]. The forces in Equation 1 are further specified as follows

$$\boldsymbol{F}_{\text{C}} = -2 \int_B \rho\,(\boldsymbol{\omega} \times \boldsymbol{v})\,\mathrm{d}V \tag{2}$$

$$\boldsymbol{F}_{\text{T}} = -\int_S \rho\boldsymbol{v}\,(\boldsymbol{v}\boldsymbol{n})\,\mathrm{d}S \tag{3}$$

$$\boldsymbol{F}_{\text{L}} = -\frac{\mathrm{d}}{\mathrm{d}t} \int_B \rho\boldsymbol{v}\;\mathrm{d}V \tag{4}$$

where ρ is the exhaust gas density, $\boldsymbol{v}$ its translational velocity and $\boldsymbol{\omega}$ the body's angular velocity with respect to the inertial coordinate system. We indicate a sub-index in the integrals to denote that these are taken over a region enclosed by a boundary. The index 'S' refers to the surface where matter leaves the system. Under the assumption of zero exhaust velocity ($\boldsymbol{v} = 0$) the forces $\boldsymbol{F}_{\text{C}}$, $\boldsymbol{F}_{\text{L}}$, and $\boldsymbol{F}_{\text{T}}$ vanish and the well-known equations of linear motion for a rigid body are obtained. However, the assumption of zero exhaust gas velocity is not valid during the thrust-phase of a launch vehicle, which is why the forces $\boldsymbol{F}_{\text{C}}$, $\boldsymbol{F}_{\text{L}}$, and $\boldsymbol{F}_{\text{T}}$ must be further considered.

Assuming constant exhaust gas density as well as constant exhaust gas velocity ($\boldsymbol{v} = $ const.) and orthogonal uniform exhaust gas particle motion over the entire nozzle exit plane ($\boldsymbol{v} = \boldsymbol{u}$), the thrust force can be simplified to

$$\boldsymbol{F}_{\text{T}} = -\|\dot{m}\|\,\boldsymbol{u} \tag{5}$$

with the total mass flow rate $\dot{m}$.

Using Reynold's transport theorem as described in [6], the Coriolis term in Equation 2 can be expanded to

$$\boldsymbol{F}_{\text{C}} = -2 \int_B \rho\,(\boldsymbol{\omega} \times \boldsymbol{v})\,\mathrm{d}V = -2\boldsymbol{\omega} \times \frac{\mathrm{d}}{\mathrm{d}t} \int_B \rho\boldsymbol{r}\;\mathrm{d}V - 2\boldsymbol{\omega} \times \int_S \rho\boldsymbol{r}\,(\boldsymbol{v}\boldsymbol{n})\,\mathrm{d}S = \boldsymbol{F}_{\text{C1}} + \boldsymbol{F}_{\text{C2}} \tag{6}$$

where $\boldsymbol{r}$ is the vector from an arbitrary reference point to each mass particle. Assuming that the gas flow velocity within the body is negligible, especially compared to the exhaust velocity over the exit surface, the terms $\boldsymbol{F}_{\text{L}}$ (Equation 4) and $\boldsymbol{F}_{\text{C1}}$ (Equation 6) can be disregarded [6]. For launch vehicles this seems to be a valid assumption since gas motion within the fuel tanks is low compared to the exhaust velocity of combustion products through the rocket engine's nozzle. The second term of the Coriolis force $\boldsymbol{F}_{\text{C2}}$ can be further simplified by using the CoM as reference frame for the Coriolis force ($\boldsymbol{r} = \boldsymbol{p}$), assuming constant exhaust gas density and velocity over the entire nozzle exit plane as well as an axis-symmetric flow of the gas particles. The $\boldsymbol{F}_{\text{C2}}$-term can thereby be simplified to

$$\boldsymbol{F}_{\text{C2}} = -2\,\|\dot{m}\|\,\boldsymbol{\omega} \times \boldsymbol{l}_{\text{CoM,N}} \tag{7}$$

where $\boldsymbol{l}_{\text{CoM,N}} = [l, 0, 0]^T$ is the vector from the system's CoM to the center of the nozzle exit plane.

For the translational motion of a variable-mass launch vehicle these assumptions yield the following simplified equations of motion

$$m\boldsymbol{a} = \boldsymbol{F}_{\text{ext}} + \boldsymbol{F}_{\text{C2}} + \boldsymbol{F}_{\text{T}} \tag{8}$$

with $\boldsymbol{F}_{\text{T}}$ and $\boldsymbol{F}_{\text{C2}}$ being described by Equations 5 and 7.

2.3 Rotational Motion

The rotational motion of a body with variable-mass can be described by the following equation provided in [6]

$$I\dot{\omega} + \omega \times I\omega = M_{\text{ext}} + M_{\text{C}} + M_{\text{H}} + M_{\text{T}} \tag{9}$$

where $I = \text{diag}(I_{xx}, I_{yy}, I_{zz})$ is the body's moment of inertia, ω and $\dot{\omega}$ are the angular velocity and acceleration, M_{ext} are external moments acting on the body, M_{C} is the Coriolis moment, M_{H} a moment due to the system's decrease in angular momentum inside its boundary (e.g. due to particle motion within the system), and M_{T} is the thrust moment. The moments in Equation 9 can further be defined as

$$M_{\text{C}} = -2 \int_B \rho \left[p \times (\omega \times v) \right] \, \mathrm{d}V \tag{10}$$

$$M_{\text{H}} = -\frac{\mathrm{d}}{\mathrm{d}t} \left(\int_B \rho (p \times v) \, \mathrm{d}V \right) \tag{11}$$

$$M_{\text{T}} = -\int_S \rho (p \times v)(vn) \, \mathrm{d}S. \tag{12}$$

The thrust moment M_{T} originates from the relative loss of angular momentum across the system boundary for a misaligned or deflected engine. Within the following investigations thrust misalignment and thrust deflections for control purposes are neglected resulting in zero thrust moment and any additional moments are summarized in the M_{ext}-term. Equation 9 reduces to the rigid body rotational equations of motion if particle velocity inside and over the boundary is zero. Since Equations 10 and 11 are quite complex, further simplifications can be considered before implementing the variable-mass system explicitly in a dynamics simulator.

Under the assumption that the fluid flow has reached steady state, which is a valid assumption for a rocket engine during nominal operation, the term M_{H} vanishes. The Coriolis moment M_{C} can be further expanded into

$$M_{\text{C}} = -\left[\frac{\mathrm{d}I}{\mathrm{d}t}\omega + \int_B \rho \left[p \times (\omega \times p) \right] (vn) \, \mathrm{d}S + \int_B \rho \left[\omega \times (p \times v) \right] \mathrm{d}V \right]. \tag{13}$$

The first term of Equation 13 captures the moment generated by the change in MoI. Since the moment of inertia changes as soon as mass leaves the system, this effect cannot be neglected. When assuming axis-symmetric motion of the fluid particles and negligible internal flow (no whirling motion), the third term of Equation 13 vanishes and can be neglected as stated in [9]. The second term, also called jet-damping term, strongly depends on the shape of the variable-mass body and the surface through which mass leaves the system. Since for rockets mass usually leaves through the nozzle exit plane, mainly the longitudinal dimensions and the nozzle geometry determine the jet-damping moment. For the implementation in a dynamics simulator the jet-damping term has to be further simplified. Therefore, an axis-symmetric flow of the exhaust gases and a nozzle aligned along the rocket's longitudinal axis is assumed. The surface integral of the jet-damping term can then be expressed in polar coordinates as

$$\int_B 1 \, \mathrm{d}S = \int_{\theta=0}^{2\pi} \int_{r=0}^{R_{\text{N}}} r \, \mathrm{d}r \, \mathrm{d}\theta \tag{14}$$

and the vector p as

$$p = \left[-l \,,\; r\cos(\theta) \,,\; r\sin(\theta) \right]^T \tag{15}$$

where l is the vector from the system's CoM to the middle of the nozzle exit plane and R_N is the radius of the nozzle exit surface as shown in Figure 2. Consequently, the jet-damping term in Equation 13 can be simplified to

$$M_{\text{jet}} = \int_B \rho \left[p \times (\omega \times p) \right] (vn) \, \mathrm{d}S = -\dot{m} \begin{bmatrix} \frac{1}{2}R_{\text{N}}^2 \\ l^2 + \frac{1}{4}R_{\text{N}}^2 \\ l^2 + \frac{1}{4}R_{\text{N}}^2 \end{bmatrix} \omega. \tag{16}$$

Finally, the simplified equations of rotational motion can be expressed as [6]

$$I\dot{\omega} + \omega \times I\omega = M_{\text{ext}} + M_{\text{Idot}} + M_{\text{jet}} \tag{17}$$

with M_{jet} being defined by Equation 16 and the moment introduced by the change in inertia defined as

$$M_{\text{Idot}} = \frac{\mathrm{d}I}{\mathrm{d}t}\omega. \tag{18}$$

As shown in this section, variable-mass modeling does not only include the obvious changes in MCI properties, but may also include additional dynamical effects. Furthermore, all additional variable-mass dynamical effects depend on the angular velocity ω. If the body under consideration does not rotate, the variable-mass dynamical effects vanish and the Newton-Euler equations of motion for a rigid body are obtained. The same applies if there is no mass flow $\dot{m}$ over the boundary of the system. There are situations when the moment of inertia changes although the mass flow is zero (e.g. stage separation). In these cases the $\boldsymbol{M}_{\text{Idot}}$-term only vanishes if the angular velocity is also zero. However, almost all launch vehicles perform some rotational maneuvers during a powered phase on their trajectory.

The effect of these additional variable-mass terms on the MCI properties and the rotational motion of a variable-mass cylinder will be discussed in Section 4, while the multi-body implementation of variable-mass systems in closed form in a multi-physics environment will be presented in the following section.

3. Multi-Body Implementation of Variable-Mass Systems

The variable-mass implementations within this work are based on the MATLAB physical modeling toolboxes Simscape and Simscape Multibody [13–15]. Simscape allows to model multi-domain physical systems in Simulink and provides the fundamental building blocks for different physical domains such as electrical, hydraulic, mechanical, thermal, and more. In contrast to Simulink, Simscape is based on acausal signal flows and physical connections that exchange energy through their bidirectional connection ports [13] like in MODELICA [16]. Simscape Multibody is a toolbox extending Simscape to multi-body simulations of three-dimensional mechanical systems using predefined body blocks, joints, sensors, etc. from which the corresponding differential algebraic equations (DAEs) are obtained [13]. Further information on Simscape and Simscape Multibody can be obtained in [13, 14].

Although Simscape allows for acausal and multi-physics dynamical modeling, the toolbox Simscape Multibody is closed–source and thus not allowing for the creation of custom multi-body components in contrast to MODELICA. This constraint can affect the architecture of a simulator in the sense that dynamical effects have to be computed and assembled on a graphical level, sometimes introducing coupling problems. An efficient and rapid simulator in Simscape can be realized when all quantities are implemented with physical Simscape interconnections. However, this can be particularly challenging when using custom components and functionalities in MATLAB and Simulink. For this reason, the multi-body implementation of variable-mass systems in Simscape Multibody currently uses interconnections of physical signals and common Simulink signals, whereby Simulink implementations were used wherever custom components or functionalities were required.
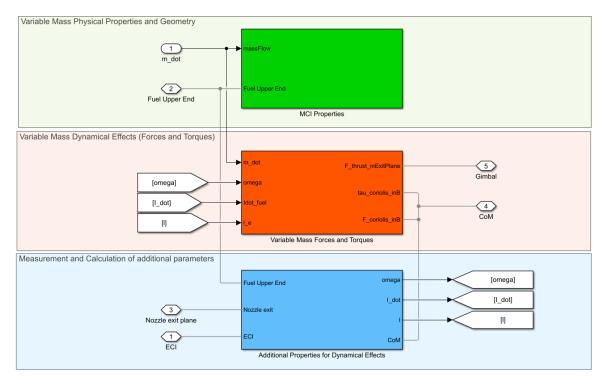

Figure 3: Variable-mass implementation in Simscape

The variable-mass system implementation is divided into three main blocks as shown in Figure 3, where each

block fulfills one main functionality. For instance, the first (green) block contains the implementation of MCI properties, whereas the second (red) block computes forces and moments due to the additional variable-mass dynamical effects as described in Sections 2.2 and 2.3. Within the third (blue) block, parameters required for the computation of the corresponding additional forces and moments are measured and calculated. This includes for example the angular velocity (`omega`), the change in MoI (`I_dot`) and the vector between CoM and nozzle exit plane (`l`). Physical, acausal ports are connected by physical signals which are represented by the gray lines in Figure 3. In the following section the implementation of MCI properties and dynamical effects will be further described.

3.1 Implementation of MCI Properties

Simscape Multibody provides variable-mass body elements where geometric parameters such as radius, length, and mass can be specified by physical signal inputs. Two different types of Simscape variable-mass elements, namely the `Variable Cylindrical Solid` and `General Variable-Mass` blocks as shown in Figure 4, are used depending on the burn type. The `Variable Cylindrical Solid` block is used for modeling the Uniform burn, End burn and Centripetal burn profiles. As inputs to this block, the current mass, length, and radius of the cylinder are required. The current mass can be calculated as the difference of initial mass and the total mass depleted over the boundary of the system which corresponds to the mass of fuel and oxidizer burned at this instant in time. This fuel and oxidizer mass is either directly given by the integral over their mass flow rates or can be determined by the engine's thrust force. Radius and length of the variable-mass cylinder are calculated analytically according to the equations in the second column of Table 1. These quantities were calculated using normal Simulink signals and `MATLAB functions` and converted to physical signals using `Simulink-PS Converters`. For the modeling of the Centrifugal burn profile the Simscape `Variable Cylindrical Solid` does not offer enough flexibility which is why the `General Variable-Mass` block is used. As inputs, the current mass and MoI are required. For the calculation of the MoI the analytical equations of Table 1 are used.
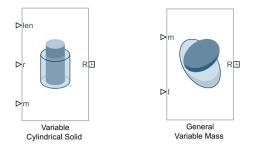

Figure 4: Simscape variable-mass elements used for variable-mass physical implementation

3.2 Implementation of Dynamical Effects

The implementation of variable-mass systems using Simscape native variable-mass elements can be seen as a variant similar to the principle of solidification. The Simscape elements from Figure 4 calculate the mass properties which include mass, MoI, and CoM based on the physical inputs for their geometric properties. At every simulation step the variable-mass element is represented by a constant mass element with the MCI properties at that instant in time. But in contrast to the variable-mass dynamics equations derived in Sections 2.2 and 2.3, Simscape does not take additional variable-mass dynamical effects into account. Therefore, these additional variable-mass forces and moments had to be added to the native Simscape elements. Each variable-mass dynamical effect as described by Equations 5, 7, 16 and 18 was implemented as a `MATLAB function` and introduced to the multi-body system by using the Simscape `External Force and Torque` block. Additional quantities required for the calculation of dynamical effects are measured using the Simscape `Transform Sensor` and `Inertia Sensor`.

One of the main challenges when implementing variable-mass dynamical effects is that they have to be applied at the CoM of the system. For variable-mass systems the CoM is usually not static but changes its position as mass or mass distribution change. Simscape on the other hand does not provide a CoM-frame where these additional forces and moments can be applied. Applying the Coriolis force resulting from variable-mass effects to a frame outside of the actual CoM of the system leads to non-physical moments and thereby to incorrect body motion. In a first approach this problem was solved by implementing an artificial CoM-frame in Simscape as shown in Figure 5. The true position of the system's CoM with respect ot a reference frame is measured using an `Inertia Sensor`. This information is then

VARIABLE–MASS DYNAMICS IMPLEMENTATION IN MULTI–PHYSICS ENVIRONMENT FOR RLV SIMULATIONS

used as a dynamical input to a `Cartesian Joint` which then moves its follower frame [14] position as provided by the input. To prevent 'degenerate mass distribution'-errors during simulation the addition of a small dummy mass to the joint's follower frame was necessary.
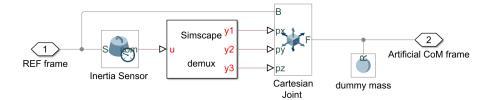

Figure 5: Implementation of an artificial CoM-frame in Simscape

The disadvantage of this implementation with an artificial CoM is a significantly increased simulation time, especially for more complex multi-body models. The initialization phase accounts for a large part of the simulation time as shown in Figure 6 where the step size is plotted over normalized simulation time. In the beginning of the simulation the solver step size is very small (see right plot in Figure 6) and increases significantly after the initialization phase but stays below its maximum values as long as there is mass flow present. The solver step size reaches its highest value and thereby the fastest solver performance when the mass flow is set to zero at $t/t_{end} \approx 0.57$. It becomes apparent that the simulation is slower in phases where mass flow is unequal to zero.
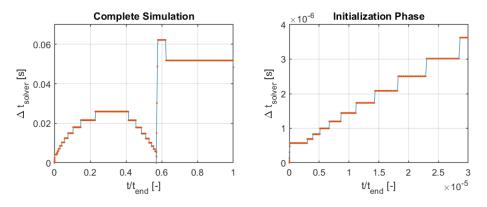

Figure 6: Solver step size for variable-mass model (with artificial CoM-frame implementation)

To circumvent the implementation of an artificial CoM and possible initialization problems the variable-mass forces and moments are applied to a fixed reference frame. The non-physical moment resulting from applying the Coriolis force outside the CoM is counteracted by an additional artificial moment which is calculated as

$$M_{CA} = -F_{C2} \times r_{ref,CoM} \tag{19}$$

where $r_{ref,CoM}$ is the vector from the fixed reference frame to the system's CoM. Figure 7 shows the implementation of this counter moment in Simscape. An `Inertia Sensor` is used to measure the vector from a reference frame to the CoM. This CoM-vector and the Coriolis force F_{C2} are used as input to a `MATLAB function` which calculates the counter moment according to Equation 19. This moment is introduced to the physical multi-body system by an `External Force and Torque` block which applies the external moment on the reference frame.
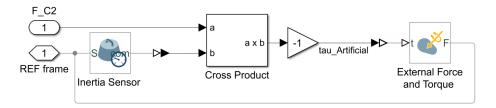

Figure 7: Implementation of an artificial counter moment

8

4. Analysis and Discussion of Results

Within this section we will show the results of the variable-mass implementation regarding the influence of variable-mass effects on the MCI properties and the rotational dynamics. The last part of this section discusses the validation against literature [6]. The results for all burn profiles using a common set of initial values will be provided in the Appendix. Since the Inverse End burn is similar to the conventional End burn just with a different orientation we will only consider the conventional End burn profile in this section. The models for all burn types within this section consist of a 'fuel-only' variable-mass element with no additional mass or inertia for structure. The nozzle was modeled with geometric properties (length, radius) but was given no mass or inertia. Furthermore, a constant mass flow through the nozzle with a constant exhaust velocity parallel to the longitudinal axis was assumed as discussed in Section 2.

4.1 Variable-Mass Effects on MCI Properties

Figure 8 displays the change in MCI properties for a variable-mass cylinder described previously. The ratio $1 - m/m_0$ is shown on the x-axis where $1 - m/m_0 = 0$ corresponds to the initial state with no fuel burned and $1 - m/m_0 = 1$ applies when all fuel is burned. Due to the constant mass flow the system's overall mass decreases linearly (top left plot). For the End burn profile this leads to a shift in the CoM due to the longitudinal change in mass distribution (top right plot). For the other burn profiles the CoM position remains constant due to the uniform loss of mass along the longitudinal axis.
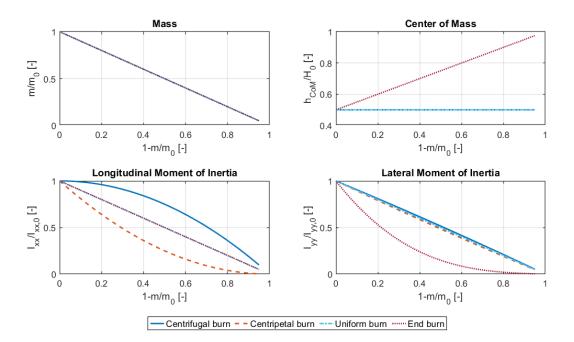

Figure 8: MCI variable-mass properties of different burn types

The changes in MoI as shown by the two lower plots are less intuitive. While for most launch vehicle simulators the change in MoI is often linearly approximated between some few MoI data points obtained for instance from CAD analysis, it can be seen that a linear approximation is often not accurate enough to describe the dynamics of the MoI, especially for the longitudinal MoI in case of Centripetal- and Centrifugal burn (bottom left plot) and the lateral MoI in case of the End burn profile (bottom right plot). However, it must be kept in mind that the models for all burn types within this investigation consist of a 'fuel-only' variable-mass element with no additional dry mass. For a complete launch vehicle model the MCI properties will change slightly different to the results shown here. This will become particularly evident in the motion of the overall CoM which then depends on the depleting propellant's CoM and the dry mass distribution. However, the cylinder problem is a useful example since it presents typical rocket-type systems in a simple and tractable way.

4.2 Variable-Mass Effects on Rotational Dynamics

Within this section the variable-mass effects on the rotational dynamics will be discussed. The translational dynamics is also influenced by variable-mass effects as it can be seen from Equation 8 where the thrust force F_T and Coriolis force F_{C2} are the main contributors. However, the impact of the Coriolis force is small compared to the thrust force [17] whose effect is well-known. Therefore, we will focus mainly on the results showcasing the influence of variable-mass effects on the rotational dynamics.

Figure 9 shows eight individual simulations with four different burn types and two initial values for the angular velocities. The results on the left show the angular velocity around the cylindrical body's longitudinal axis when the angular velocity is initialized as $\omega_0 = [\omega_{x0}\ 0\ 0]^T$ with $\omega_{x0} \neq 0$. If no variable-mass dynamical effects are applied, the angular velocity will remain constant as it is also the case for the Uniform and the End burn profiles. With radial burn profiles, including the Centrifugal burn and the Centripetal burn, the longitudinal angular velocity does not remain constant but is first amplified and with decreasing mass attenuated for the Centripetal burn, and vice-versa for the Centrifugal burn, if the angular velocity is not zero. The results on the right showcase the angular velocity around the
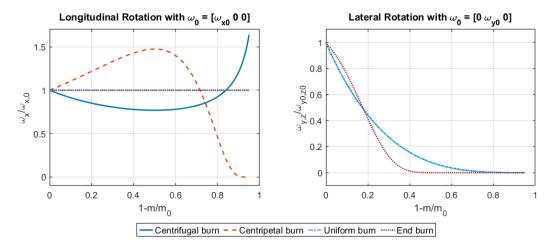
Figure 9: Longitudinal and lateral angular velocities for different burn types and initial conditions

cylindrical body's lateral axes when the angular velocity is initialized as $\omega_0 = \begin{bmatrix} 0\ \omega_{y0}\ \omega_{z0} \end{bmatrix}^T$ with either $\omega_{y0} \neq 0$ or $\omega_{z0} \neq 0$. It can be shown that all burn types have an attenuating effect on the rotational dynamics. However, the angular velocity would remain constant if no variable-mass dynamical effects would be considered.

These simple examples illustrate the impact of variable-mass dynamical effects on the rotational dynamics of cylindrical bodies and it becomes evident, that neglecting these effects may result in significantly different dynamics. For the investigations within this section a radius to length ratio of $(2R_0/L_0 = 0.15)$ was used which represents common ratios of launch vehicles (Vega - 1st stage: $2R_0/H_0 \approx 0.27$, Vega - 3rd stage: $2R_0/H_0 \approx 0.46$ [20]). As it will be shown in Section 4.3, the radius to length ratio has a significant impact on the variable-mass dynamical effects, especially for the lateral rotation of radial burn types. For typical geometric ratios of launch vehicles Table 2 adequately summarizes the variable-mass effects of the different burn types.

Table 2: Variable-mass dynamical effects on lateral and longitudinal motion for all burn types with $(2R_0/L_0 = 0.15)$

Direction	Uniform Burn	End Burn	Centrifugal Burn	Centripetal Burn
Longitudinal	None	None	Attenuating, then amplifying	Amplifying, then attenuating
Lateral	Attenuating	Attenuating	Attenuating	Attenuating

For further investigation of the variable-mass effects, the resulting moments were assessed as shown in Figure 10 for the longitudinal rotation of a Centrifugal burn type cylinder. In this case, the fuel burn lasts for approximately 11 seconds. From left to right, the figure shows the evolution of mass, angular velocity and resulting variable-mass moments. As mass decreases, the angular velocity is first attenuated and later amplified as already seen in Figure 9. This change in angular velocity is caused by the variable-mass dynamical effects, namely the jet-damping moment and

moment due to the change in MoI as described by Equations 16 and 18. For this burn type M_{Idot} has an amplifying, while M_{jet} has an attenuating effect. Initially, M_{jet} predominates the variable-mass effects due to its dependency on geometrical properties, resulting in the initial attenuation of the angular velocity. Since M_{Idot} is determined by the change in MoI as defined in Table 1, the amplitude of M_{Idot} increases as the inner radius increases which causes the overall variable-mass effect to reverse. Figures 17 and 18 in the Appendix show the variable-mass moments for all burn types. As evidenced in that figures, the jet-damping moment was the decisive quantity for the lateral angular velocities while both moments had a decisive share on the longitudinal angular velocity, canceling each other out for the Uniform and End burn configuration.
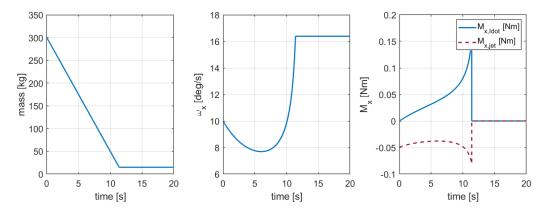

Figure 10: Variable-mass simulation for longitudinal rotation of a Centrifugal burn type cylinder

Additionally, the ratio of the nozzle radius to the cylinder radius also has an influence on the variable-mass dynamical effects (see Equation 16). The larger the nozzle radius, the higher is the resulting jet-damping moment and its attenuating effect.

All results within this section have been cross-checked and validated against alternative implementations using the multi-physics and acausal modeling language MODELICA [16] and its simulation environment DYMOLA [5]. A verification against literature [6] is shown in the next sub-section.

4.3 Validation Against Literature [6]

In this section we will focus on the validation of the variable-mass implementation for all burn types against [6]. We will focus this validation in terms of the attitude motions of a variable-mass cylinder with initial angular velocity as explained in [6]. Similar to previous sections, a 'fuel-only' variable-mass cylinder with no additional mass or inertia for structure and nozzle was used for the investigations. The fuel was modeled as a cylinder open on one side where mass is able to leave the system. In contrast to the previous sections, this corresponds to a nozzle with zero length and a radius of $R_N = R_0$. A constant mass flow through the nozzle with a constant exhaust velocity parallel to the longitudinal axis was assumed. For the comparison an initial angular velocity either in longitudinal or lateral direction was applied (Note: while in [6] the longitudinal- or spin-axis is defined to be the body's z-axis we used the flight dynamics convention for launch vehicles and assigned the longitudinal axis to the body's x-axis as shown in Figure 1 and 2). For the validation we only discuss the comparison of the lateral rotation of the Centrifugal burn profile as shown in Figure 11. The comparison of other burn types as well as longitudinal rotation results can be found in the Appendix in Figures 12, 13, 15 and 16.

Figure 11 shows the change of angular velocity for the Centrifugal burn type as the system loses mass. Good agreement between literature and Simscape implementation results indicates a correct implementation in the multi-body environment. Figure 11 also depicts the dynamics of the angular velocity for different ratios of initial cylinder radius R_0 to initial cylinder length H_0. Depending on this ratio, the variable-mass dynamics can either have an attenuating or amplifying effect. A ratio of $2R_0/H_0 \approx 1.63$ divides the stable region from the unstable region. Since launch vehicle systems tend to have smaller ratios an attenuating effect of the variable-mass dynamics in case of a Centrifugal burn is expected for lateral rotations. A similar effect can be observed for Centripetal burn profiles where below a ratio of $2R_0/H_0 \approx 1.63$ lateral angular velocities are directly attenuated while for higher ratios angular velocities are amplified in the beginning of the burn and attenuated after some mass is depleted (see Figure 13 in the Appendix).
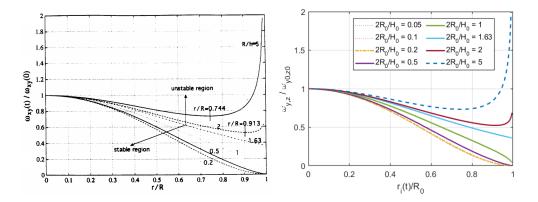
11

Figure 11: Centrifugal burn: results from literature (left) [6] and Simscape implementation (right) for lateral rotation

4.4 Summary on Variable-Mass Dynamical Effects

A summary of the key take-aways for variable-mass dynamical systems can be stated as:

- Linearity of the changes in moment of inertia and center of mass shall not be always assumed, especially since this does not hold true for certain burn profiles (recall Figure 8).

- Variable-mass dynamical effects (more precisely the Coriolis moment and force under consideration) only occur in the presence of an angular velocity. If there is zero angular velocity, the equations of motion simplify to the rigid body dynamics with changing mass and inertia properties.

- Variable-mass effects due to the jet-damping moment M_{jet} and the F_{C2}-force depend strongly on the exhaust gas velocity as well as the vehicle and nozzle geometric properties. In particular they both depend on the distance between the vehicle's center of mass and the nozzle exit plane while the jet-damping moment additionally depends on the nozzle exit radius. For the jet-damping term, all three directions depend on the nozzle-radius while only the lateral shares depend on the distance between the vehicle's center of mass and the nozzle exit plane.

- The magnitude of the Coriolis force F_{C2} is small compared to the magnitude of the thrust force F_T. In case of an axis-symmetric rocket (with one nozzle) there is no Coriolis force in the vehicle's longitudinal axis.

- Variable-mass dynamical effects may have an attenuating or amplifying effect on the vehicle's angular velocities. The effect depends strongly on the burn type as well as the vehicle and nozzle geometric properties. Within the test cases of this document the influence of the variable-mass effects on the angular velocity of a cylinder with a radius to length ratio adequate for common launch vehicles were assessed as summarized in Table 2. This may differ for more realistic vehicles with structural mass and inertia or vehicles with different geometrical properties.

- Coriolis moments, namely the jet-damping moment M_{jet}, and the moment due to the change in moment of inertia M_{Idot} act in different directions. Due to the geometry assumed in this paper, the jet-damping moment was the decisive quantity for the transversal angular velocities while both moments had a decisive share on the longitudinal angular velocity, canceling each other out for the Uniform burn and the End burn configurations. This effect varies for different vehicle geometries. In particular a change in the nozzle radius can have a significant effect here.

- Even though most dynamics simulators in literature do not account for variable mass dynamical effects they are successfully used for G&C design and validation of real missions. Several factors are assumed to contribute to this. The variable-mass dynamical effects within this section are shown for a 'fuel-only'-configuration with no additional inertia for structure, nozzle etc. The impact on a realistic launch vehicle model is less than for the 'fuel-only'-configuration. Additionally, the variable mass effects linearly depend on the angular velocity which is usually low, especially in lateral direction. This all results in low magnitudes for the variable-mass forces and moments. At last, the real vehicle runs in closed-loop control with the controller designed to cope with external disturbances M_{ext} coming from aerodynamics, mass-uncertainties, wind etc. which are generally much higher than the variable-mass effects. The attenuating action of M_{jet} demonstrated in Section 4.2 is then provided by the controller instead, which also immediately acts against amplifying variable-mass effects.

5. Conclusion

The objective of this paper was to present a Simscape® implementation and verification of variable-mass dynamics towards the preliminary design and development of the dedicated multi-physics simulator R2M2 (Rapid Reusable Launcher Simulation via Multi-physics Modelling). A comparison with results from literature and a cross-check with simulation results using MODELICA show good accordance of the variable-mass implementation results in Simscape. Variable-mass dynamical effects which are often neglected in launch vehicle simulators were shown to have a noticeable effect on the overall system dynamics, especially regarding the rotational motion. Therefore, these effects should not be neglected in the presence of angular velocities which is expected in launch vehicle dynamics and justifies the implementation of variable-mass effects within the R2M2 simulator. The investigations within this paper were performed with a 'fuel-only' variable-mass element with no additional mass or inertia for structure or nozzle. Further investigations with more realistic model setups including structure and multiple nozzles will be performed to show the impact of variable-mass dynamical effects on more realistic launch vehicle models with the overall goal to implement multi-physics launch vehicle models in the R2M2 simulator.
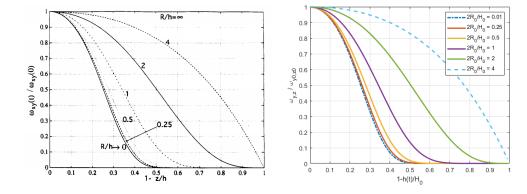
Acknowledgments

References

[1] P. Acquatella B. Launch Vehicle Multibody Dynamics Modeling Framework for Preliminary Design Studies. In *6th International Conference on Astrodynamics Tools and Techniques (ICATT)*, 2016.

[2] P. Acquatella B., L. E. Briese, and K. Schnepper. Guidance command generation and nonlinear dynamic inversion control for reusable launch vehicles. *Acta Astronautica*, 174, 2020.

[3] L. E. Briese, P. Acquatella B., and K. Schnepper. Multidisciplinary modeling and simulation framework for launch vehicle system dynamics and control. *Acta Astronautica*, 170, 2020.

[4] L. E. Briese, K. Schnepper, and P. Acquatella B. Advanced Modeling and Trajectory Optimization Framework for Reusable Launch Vehicles. In *IEEE Aerospace Conference*, 2018.

[5] DYMOLA. *Version 2022*. Vélizy-Villacoublay, France, Dassault Systèmes, 2022.

[6] F. O. Eke. Dynamics of Variable Mass Systems. Technical Report CR-1998-208246, National Aeronautics and Space Administration (NASA), 1999.

[7] F. O. Eke and T. C. Mao. On the dynamics of variable mass systems. *International Journal of Mechanical Engineering Education*, 2000.

[8] F. O. Eke and J. Sookgaew. Influence of Propellant Burn Pattern on the Attitude Dynamics of a Spinning Rocket. *Nonlinear Dynamics and Systems Theory*, 5(3), 2005.

[9] F. O. Eke, T. Tran, and J. Sookgaew. Dynamics of a Spinning Rocket with Internal Mass Flow. *Nonlinear Dynamics and Systems Theory*, 6(2), 2006.

[10] F. O. Eke and S.-M. Wang. Attitude Behavior of a Variable Mass Cylinder. *Journal of Applied Mechanics*, 1995.

[11] B. Gäßler, P. Acquatella B., C. Yábar Vallès, A. Rinalducci, and S. Bennani. Preliminary Design and Development of MAST, a Multivehicle Analysis and Separation Tool. In *8th International Conference on Astrodynamics Tools and Techniques (ICATT)*, 2021.

[12] T. C. Mao and F. O. Eke. Attitude Dynamics of a Torque-Free Variable Mass Cylindrical Body. *The Journal of the Astronautical Sciences*, 2000.

[13] MathWorks. Simscape Documentation, 2022.

[14] MathWorks. Simscape Multibody Documentation, 2022.

[15] MATLAB. *Version R2021b*. Natick, Massachusetts, United States, The Mathworks, Inc., 2021.

[16] Modelica Association. *Modelica - A Unified Object-Oriented Language for Physical Systems Modeling, Language Specification Version 3.4*, 2017. Version 3.5.

[17] E. Mooij. The Motion of a Vehicle in a Planetary Atmosphere. Technical Report LR-768, Delft University of Technology, 1994.

[18] A. Nanjangud. Geometry of motion and nutation stability of free axisymmetric variable mass systems. *Nonlinear Dynamics*, 2018.

[19] P. Simplício. *Guidance and Control Elements for Improved Access to Space: from Planetary Landers to Reusable Launchers*. PhD thesis, Department of Aerospace Engineering, Bristol Doctoral College.

[20] E. Perez. Vega - User's Manual Issue 4. Technical report, Arianespace, 2014.

[21] M. J. Reiner and J. Bals. Nonlinear inverse models for the control of satellites with flexible structures. In *Proceedings of the 10th International Modelica Conference*, 2014.

[22] P. Simplício and S. Bennani. Worst-case Launch Vehicle Stage Separation Analysis. 2015. 3rd CEAS Specialist Conference on Guidance, Navigation and Control, 2015.

[23] P. Simplício, A. Marcos, and S. Bennani. Reusable Launchers: Development of a Coupled Flight Mechanics, Guidance, and Control Benchmark. *Journal of Spacecraft and Rockets*, 57(1), 2020.

[24] J. Sookgaew and F. O. Eke. Effects of Substantial Mass Loss on the Attitude Motions of a Rocket-Type Variable Mass System. *Nonlinear Dynamics and Systems Theory*, 4(1), 2004.

VARIABLE–MASS DYNAMICS IMPLEMENTATION IN MULTI–PHYSICS ENVIRONMENT FOR RLV SIMULATIONS

Appendix

Validation Against Literature [6] - Additional Plots

Figure 12: End burn: Results from literature (left) [6] and Simscape implementation (right) for lateral rotation
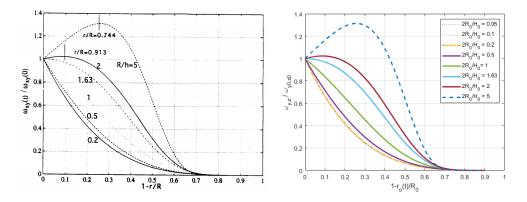
Figure 13: Centripetal burn: Results from literature (left) [6] and Simscape implementation (right) for lateral rotation
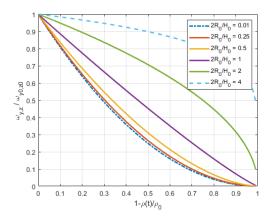
Figure 14: Uniform burn: Results from Simscape implementation for lateral rotation (no literature results available)

VARIABLE–MASS DYNAMICS IMPLEMENTATION IN MULTI–PHYSICS ENVIRONMENT FOR RLV SIMULATIONS
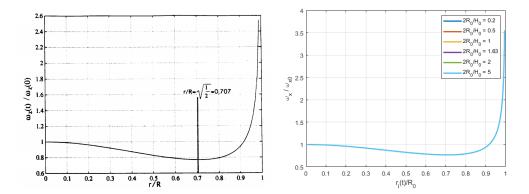

Figure 15: Centrifugal burn: Results from literature (left) [6] and Simscape implementation (right) for longitudinal rotation (Note that all lines are overlapped)
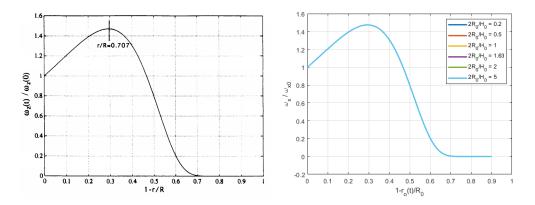

Figure 16: Centripetal burn: Results from literature (left) [6] and Simscape implementation (right) for longitudinal rotation (Note that all lines are overlapped)

VARIABLE–MASS DYNAMICS IMPLEMENTATION IN MULTI–PHYSICS ENVIRONMENT FOR RLV SIMULATIONS
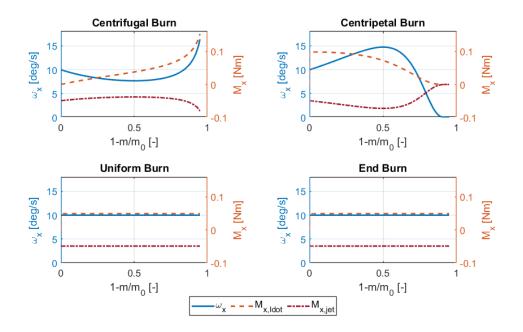
Variable-Mass Moments for all Burn Types

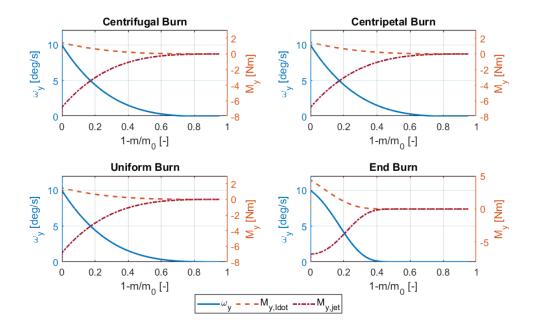Figure 17: Longitudinal variable-mass moments for all burn types

Figure 18: Lateral variable-mass moments for all burn types